interested in studying the nonequilibrium micellar state, because many studies involving the interactions of oppositely charged dyes and surfactants may have been made on nonequilibrium states. As we show in the present papers, the properties of the aggregates may depend on their past history, including the method of preparation and the time of aging, so the diversity of opinion regarding the nature of the aggregates should not be surprising (references cited in ref 2). Our results are reproducible when we use the specified methods, but we are dealing with metastable states on the time scale of most of our observations. We have shown that the properties of the metastable state can be governed by the route to the state.

When our dispersions are prepared at a dye concentration of 2.5×10^{-5} M and at low S/D ratios, the solubility product of the dye-CTAB salt is exceeded and the formation of crystallites (thermodynamic state) can compete to a small extent with micelle formation (kinetic state).[2] Once the micelles are formed, equilibration is very slow. The light-scattering intensity from the micellar solutions at low S/D ratios is greater than that from solutions containing CTAB at concentrations near the cmc, so the number of micelles or the micellar molecular weights in the very dilute solutions must be appreciable and must account for most of the ester present. Under these conditions the concentrations of monomeric ester must be less than the solubility product for the salts so that growth of new crystal nuclei probably does not occur from the bulk solution but by reorientation within the mixed micelles.

Acknowledgment. Technical assistance by Shelley Harkaway is gratefully acknowledged.

References and Notes

(1) R. L. Reeves, R. S. Kaiser, and H. W. Mark, *J. Colloid Interface Sci.*, **45**, 396 (1973).
(2) R. L. Reeves, *J. Am. Chem. Soc.*, **97** (1975), preceding paper.
(3) C. Tanford, "The Hydrophobic Effect", Wiley, New York, N.Y., 1973, Chapter 8.
(4) L. R. Romsted and E. H. Cordes, *J. Am. Chem. Soc.*, **90**, 4404 (1968).
(5) F. Helfferich, "Ion Exchange", McGraw-Hill, New York, N.Y., 1962, p 169.
(6) E. W. Anacker, "Cationic Surfactants", Marcel Dekker, New York, N.Y., 1970, p 257.
(7) C. A. Bunton and L. Robinson, *J. Org. Chem.*, **34**, 773, 780 (1969).
(8) J. Baumrucker, M. Calzadilla, M. Centeno, G. Lehrmann, M. Urdaneta, P. Lindquist, D. Dunham, M. Price, B. Sears, and E. H. Cordes, *J. Am. Chem. Soc.*, **94**, 8164 (1972).
(9) Reference 5, Chapter 5.
(10) C. A. Bunton, M. Minch, and L. Sepulveda, *J. Phys. Chem.*, **75**, 2707 (1971).
(11) C. A. Bunton, M. J. Minch, J. Hidalgo, and L. Sepulveda, *J. Am. Chem. Soc.*, **95**, 3262 (1973).
(12) G. C. Kresheck, E. Hamori, G. Davenport, and H. A. Scheraga, *J. Am. Chem. Soc.*, **88**, 246 (1966).
(13) B. C. Bennion, L. K. J. Tong, L. P. Holmes, and E. M. Eyring, *J. Phys. Chem.*, **73**, 3288 (1969).
(14) T. Yasunaga, K. Takeda, and S. Harada, *J. Colloid Interface Sci.*, **42**, 457 (1973).
(15) N. Muller, *J. Phys. Chem.*, **78**, 3017 (1972).
(16) H. Peper and E. G. Taylor, *J. Colloid Sci.*, **18**, 318 (1963).
(17) P. Becher and N. K. Clifton, *J. Colloid Sci.*, **14**, 519 (1959).
(18) T. Nash, *J. Colloid Sci.*, **14**, 59 (1959).
(19) M. Grätzel and J. K. Thomas, *J. Am. Chem. Soc.*, **95**, 6885 (1973).

Luminescence of Heterobischelated Complexes of Iridium(III). I. Resolution of the Multiple Emissions of *cis*-Dichloro-1,10-phenanthroline-5,6-dimethyl-1,10-phenanthrolineiridium(III) Chloride

Richard J. Watts,* Marty J. Brown,[1] B. G. Griffith,[1] and J. S. Harrington

Contribution from the Department of Chemistry, University of California, Santa Barbara, California 93106. *Received January 6, 1975*

Abstract: Luminescence decay curves of *cis*-dichloro-1,10-phenanthroline-5,6-dimethyl-1,10-phenanthrolineiridium(III) chloride have been determined as a function of emission wavelength. A two-level model has been used to decompose each decay curve into a sum of two exponentials with lifetimes of 9.5 and 65 μsec. From this analysis, the total emission spectrum has been decomposed into two component spectra. The levels giving rise to these spectra are split by 200–300 cm^{-1}, and appear to arise from $d\pi^*$ and $\pi\pi^*$ orbital parentage. Analysis of luminescence decay curves as a function of excitation wavelength indicates that upper states of $d\pi^*$ parentage tend to feed the $d\pi^*$ emission and states of $\pi\pi^*$ parentage feed the $\pi\pi^*$ emission. On the basis of these results we suggest the following selection rules for radiationless transitions in heavy-metal complexes: $d\pi^* \leftrightarrow d\pi^*$; $\pi\pi^* \leftrightarrow \pi\pi^*$; $d\pi^* \nleftrightarrow \pi\pi^*$.

Numerous studies of energy transfer processes among the electronic excited states of highly symmetrical complexes of d^6 metal ions at 77 K suggest that radiationless transitions from upper electronic excited states to the lowest excited state occur with nearly 100% efficiency.[2a] Experimental evidence now indicates that this "lowest excited state" is often a manifold of thermally equilibrated levels which are split by energies of less than kT.[2b] Studies of photochemical processes in highly symmetrical complexes of d^6 metal ions also indicate that the lowest excited state is often responsible for the photochemical activity regardless of which state is initially excited.[3] There is, however, mounting evidence that the lowest excited state of some d^6 heavy-metal complexes is not always populated with 100% efficiency.[3] Studies of both photochemical[4] and photophysical[5] energy transfer processes in certain Rh(III) complexes suggest that the lowest excited states may not be efficiently coupled to higher states by radiationless processes. Preliminary studies of photophysical energy transfer processes in complexes of Ir(III) with low symmetry also suggest that electronic excited states may not be coupled to one another via radiationless pathways in these systems.[6]

Although the occurrence of light emission from several nonequilibrated states of heavy-metal complexes is a rather

Table I. Nonlinear Least-Squares Fit of Luminescence Decay Curves of $[IrCl_2(phen)(5,6\text{-mephen})]Cl$ as a Function of Emission Wavelength[a,b]

Emission wavelength, nm	$B(\nu)/A(\nu)$	Emission wavelength, nm	$B(\nu)/A(\nu)$
474	1.32	525	1.12
476	1.30	530	1.37
478	0.925	540	3.30
480	0.110	550	4.10
482	0.486	560	2.36
484	0.371	570	2.15
486	0.338	580	3.91
488	0.283	590	6.90
490	0.254	600	5.75
492	0.356	610	5.18
500	1.61	620	7.63
510	3.12	630	10.2
520	1.39		

[a] Fit according to eq 1 with τ_a = 9.5 μsec and τ_b = 65 μsec. [b] Measured in ethanol–methanol (4:1 v/v) at 77 K.

rare occurrence, several features appear to be associated with the phenomenon. In studies of multiple emission from heterotrischelated complexes of Rh(III) with 1,10-phenanthroline (phen) and 2,2′-bipyridine (bipy), Halper and DeArmond[5] established that their results could best be interpreted in terms of a localized exciton model. In this model the dual emission is viewed as emission of energy localized in either the phenanthroline ligand or the bipyridine ligand. Thus, the two emitting states in this case are both $\pi\pi^*$ in their orbital character.

In studies of light emission from heterobischelated complexes of Ir(III) with phen, bipy, and 5,6-dimethyl-1,10-phenanthroline (5,6-mephen), Watts[6] established that multiple emissions from thermally nonequilibrated states occur in $[IrCl_2(phen)(5,6\text{-mephen})]Cl$. However, the very slight deviations from exponential luminescence decay which were observed for $[IrCl_2(phen)(bipy)]Cl$ indicate that the electronic excited states of this complex may be close to thermal equilibration. These results suggest that $\pi\pi^*$ and $d\pi^*$ states may be sufficiently uncoupled to emit independently, but that two $d\pi^*$ states are coupled strongly enough to approach thermal equilibration. Recent studies of heterotrischelated complexes of Ru(II) appear to confirm the conclusion that $d\pi^*$ states undergo rapid thermal equilibration.[7] From these two studies it appears that $\pi\pi^*$ states tend to be much more weakly coupled to other electronic levels than are either $d\pi^*$ or d–d states. This suggests that a set of selection rules for radiationless transitions based upon the orbital nature of the electronic levels may be operative in unsymmetrical complexes.

Although previous studies of multiple emissions from heavy-metal complexes have included analyses of the resultant nonexponential luminescence decay curves, only limited information on the wavelength dependence of these decay curves has been reported. Halper and DeArmond[5] lacked sufficient sensitivity in their instrumentation to determine the wavelength dependence of the luminescence decay curves for the Rh(III) complexes. In a preliminary communication, we obtained sufficient intensity with 337-nm excitation from a pulsed nitrogen laser to determine luminescence decay curves at three different wavelengths in the emission spectra of the Ir(III) complexes which were studied.

In this paper we wish to report a complete analysis of the dependence of the luminescence decay curves of $[IrCl_2(phen)(5,6\text{-mephen})]Cl$ on the wavelength at which the emission is monitored. From this study we are able to deduce the emission spectrum of each of the luminescent states. The shapes of these spectra are confirmed by time-resolved spectral analysis of the emission via box-car averaging techniques. Furthermore, we have successfully employed a pulsed-dye laser in order to determine the dependence of the luminescence decay curves on the excitation wavelength.

Experimental Section

The synthesis and characterization of *cis*-dichloro-1,10-phenanthroline-5,6-dimethyl-1,10-phenanthrolineiridium(III) chloride have been described in a previous publication.[8] Absolute ethanol (Commercial Solvent Corp., Reagent Quality) and absolute methanol (Matheson Coleman and Bell, spectroquality) were used without further purification. Deionized water was further purified by distillation before use. Solutions of the complex were prepared in the solvent mixtures (ethanol–methanol 4:1 v/v or methanol–water 4:1 v/v) at concentrations of 10^{-3} to 10^{-4} *M*. Once prepared, the solutions were stored in dark containers under refrigeration when not in use.

Decay curve measurements were made on glasses at liquid nitrogen temperature in optical quartz dewars. The complex was excited at 337 nm with the output of an Avco C950 pulsed nitrogen laser. Excitation of the complex between 360 and 505 nm was accomplished by use of an Avco Dial-A-Line dye laser with a series of static dye cells. Decay curves were monitored at wavelengths throughout the emission spectrum with a 0.8 *M* Ebert-Fastie scanning monochromator. Slit widths of 0.2 mm (0.2 nm resolution) were employed when the complex was excited at 337 nm and 1.0 mm slits (1 nm resolution) were used with the tunable dye laser. The emission was detected with an EMI 9558 F photomultiplier whose output was applied to the vertical input of a Tektronix 549 oscilloscope through a 1 kΩ terminating resistor. The oscilloscope was externally triggered by the synchronized output signal from the laser. Pulse rates of 50–100 pps (pulses per second) were employed with 337-nm excitation. Operation of the dye laser between 360 and 505 nm required a reduction of the pulse rate to 10–20 pps. A display of the emission intensity as a function of time as well as a reference base line and time marks from a Tektronix 184 time mark generator were photographed at each wavelength with a Tektronix C-12 camera.

In order to determine time-resolved emission spectra, the output of an EMI-9558QA photomultiplier was applied to the input of the PAR Model 164 gated integrator module of a PAR Model 162 box-car averager. The average value of the intensity of the decaying emission at various times after the excitation was determined by an appropriate selection of aperture delay and duration times on the boxcar averager. Time-resolved emission spectra were generated by scanning the monochromator at a rate of 10 nm/min while monitoring the output of the box-car averager with a Soltec-Rikadenki Model B-161 strip chart recorder. With this scanning speed and the minimum pulse rate of 10 pps which we employed, the output of the box-car averager represented the average of at least 60 intensity measurements for each 1 nm segment of the spectrum.

Results

A. Dependence of Luminescence Decay Curves on Emission Wavelength. The decay curves of $[IrCl_2(phen)(5,6\text{-mephen})]Cl$ were analyzed at each emission wavelength as the sum of two exponentials. The general form of the function used in this analysis is given by eq 1, where $I(\nu,t)$ is the

$$I(\nu,t) = A(\nu)e^{-t/\tau_a} + B(\nu)e^{-t/\tau_b} \quad (1)$$

luminescence intensity as a function of time and frequency, $A(\nu)$ and $B(\nu)$ are frequency-dependent pre-exponential factors, and τ_a and τ_b are constants which are independent of the emission frequency. We will discuss the physical interpretation of the parameters $A(\nu)$, $B(\nu)$, τ_a, and τ_b at a later point. It was found that this function could be used to fit the experimental decay curves at all frequencies in the emission spectrum by assigning values of 65 μsec to τ_a and 9.5 μsec to τ_b. Values of $A(\nu)$ and $B(\nu)$ for each decay curve, which were determined by a nonlinear least-squares analysis, are listed as $B(\nu)/A(\nu)$ in Table I. Using this anal-

Table II. Nonlinear Least-Squares Fit of Luminescence Decay Curves of $[IrCl_2(phen)(5,6\text{-mephen})]Cl$ as a Function of Excitation Wavelength[a-c]

Excitation wavelength, nm	$B(\nu)/A(\nu)$	Excitation wavelength, nm	$B(\nu)/A(\nu)$
337	3.11	410	4.29
360	6.38	420	6.39
370	5.63	430	8.15
380	5.05	440	10.3
390	4.46	450	37.8
400	4.51		

[a] Fit according to eq 1 with $\tau_a = 9.5$ μsec and $\tau_b = 65$ μsec. [b] Measured in ethanol–methanol (4:11 v/v) at 77 K. [c] Emission monitored at 510 nm.

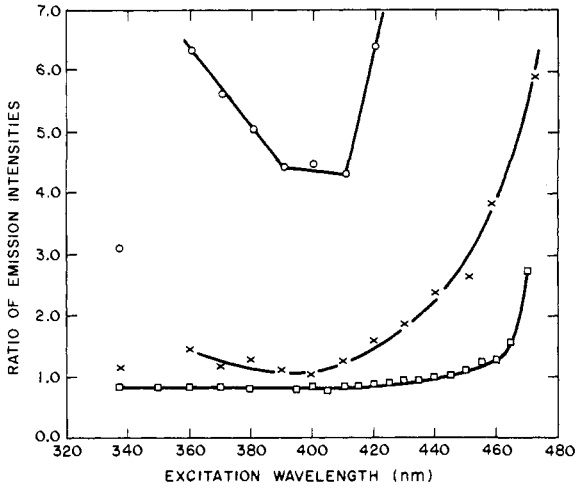

Figure 1. Some ratios of emission intensities of the two emitting levels of $[IrCl_2(phen)(5,6\text{-mephen})]Cl$ as a function of excitation wavelength: (○) $B(\nu)/A(\nu)$ from eq 1 at an emission wavelength of 510 nm; (×) ratio of emission intensities at 510 and 486 nm from time-resolved emission spectroscopy with a 2-μsec delay time; (□) ratio of emission intensities at 522 and 486 nm from time-integrated emission spectroscopy.

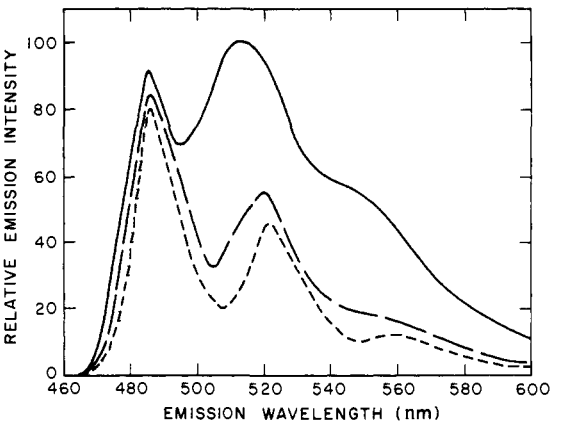

Figure 2. Emission spectra of $[IrCl_2(phen)(5,6\text{-mephen})]Cl$ excited at 337 nm in ethanol–methanol (4:1 v/v) at 77 K as a function of time: (—) emission spectrum 2 μsec after excitation; (- - -) emission spectrum 20 μsec after excitation; (- - -) emission spectrum 200 μsec after excitation.

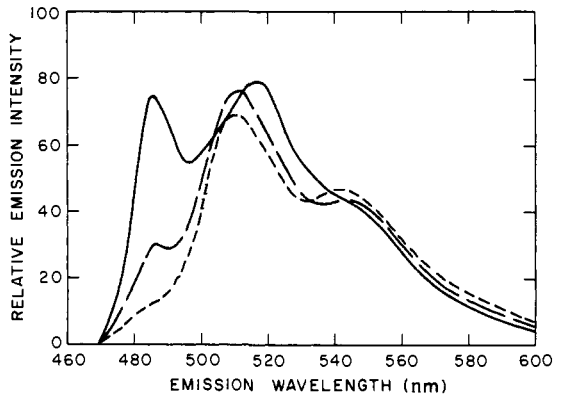

Figure 3. Time-resolved emission spectra of $[IrCl_2(phen)(5,6\text{-mephen})]Cl$ in ethanol–methanol (4:1 v/v) at 77 K as a function of excitation wavelength; (—) emission spectrum 2 μsec after excitation at 400 nm; (- - -) emission spectrum 2 μsec after excitation at 440 nm; (- - -) emission spectrum 2 μsec after excitation at 472 nm.

ysis, it was possible to fit each experimental point on the decay curves within ±10%. The largest deviations between calculated and observed data points were found to occur in the high-frequency end of the total emission spectrum, between 474 and 484 nm, which may indicate a contribution from a third component to the total luminescence in this region.

B. Dependence of Luminescence Decay Curves on Excitation Wavelength. The dependence of the luminescence decay curves of $[IrCl_2(phen)(5,6\text{-mephen})]Cl$ on excitation energy was determined for excitation wavelengths between 337 and 450 nm. The decay curves were monitored at an emission wavelength of 510 nm and were analyzed again by a nonlinear least-squares fit to eq 1 with values of 65 and 9.5 μsec for τ_a and τ_b. The ratios, $B(\nu)/A(\nu)$, obtained by this procedure are listed in Table II. Although lifetime data could be monitored at excitation wavelengths as long as 505 nm, the decay curves at wavelengths longer than 450 nm were found to contain no significant contribution from $A(\nu)$. A plot of the ratio $B(\nu)/A(\nu)$ as a function of excitation wavelength is shown in Figure 1. This figure illustrates that a peak in the ratio occurs between 337 and 370 nm and that the ratio increases rapidly at excitation wavelengths longer than 420 nm.

C. Luminescence Spectra. The time-resolved luminescence spectra of $[IrCl_2(phen)(5,6\text{-mephen})]Cl$ at several different delay times are illustrated in Figure 2. These spectra were all recorded under excitation at 337 nm. It is apparent from Figure 2 that the intensity distribution in the luminescence spectrum of this complex is strongly dependent upon time. The spectrum of emitted light 2 μsec after excitation has its maximum intensity at 515 nm with a lower intensity peak at 486 nm and a shoulder at 545 nm. At 20 μsec the peak at 486 nm carries maximum intensity. The peak in the 2-μsec spectrum at 515 nm shifts to 520 nm and the shoulder shifts from 545 to 550 nm. At 200 μsec after excitation the 486-nm peak grows further in its relative intensity and the second peak moves out to 522 nm. The shoulder which previously appeared at 545–550 nm becomes a well-resolved peak at 560 nm. At 400 μsec, which represents the limit at which we have sufficient intensity to record a spectrum, no further major changes are observed.

The dependence of the time-resolved luminescence spectra of $[IrCl_2(phen)(5,6\text{-mephen})]Cl$ on the excitation wavelength is illustrated in Figure 3. Since the long-time emission spectrum is invariant to excitation energy, only the short-time (2 μsec) spectrum is illustrated. This figure shows that there is a strong dependence of the intensity distribution in the short-time spectrum on excitation wavelength. Note that under low-energy (472 nm) excitation the prominent peak which appears at 486 nm in the short-time spectrum excited at 337 nm diminishes to a small shoulder. Also, the major peak which was found at 515 nm under 337-nm excitation is shifted to 510 nm, and the shoulder at 545 nm becomes a well-resolved peak at the same wave-

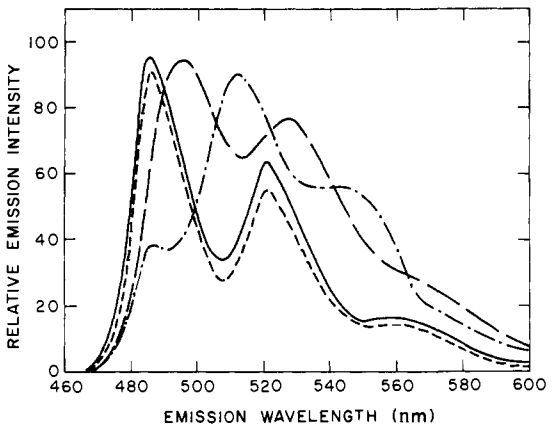

Figure 4. Solvent dependence of time-resolved emission spectra of [$IrCl_2$(phen)(5,6-mephen)]Cl: (—) emission spectrum 50 μsec after excitation at 440 nm in methanol–water (4:1 v/v) at 77 K; (– – –) emission spectrum 2 μsec after excitation at 440 nm in methanol–water (4:1 v/v) at 77 K; (- - -) emission spectrum 50 μsec after excitation at 440 nm in ethanol–methanol (4:1 v/v) at 77 K; (- · -) emission spectrum 2 μsec after excitation at 440 nm in ethanol–methanol (4:1 v/v) at 77 K.

length. As the excitation energy is increased toward 337 nm, the intensity of the peak at 486 nm begins to increase relative to the intensity at 510 nm, and the peak at 545 nm begins to broaden to a shoulder. However, the ratio of the intensity at 510 nm to the intensity at 486 nm does not decrease monotonically as the excitation energy is increased from 472 to 337 nm. The effect is illustrated in Figure 1, in which this ratio is plotted as a function of excitation wavelength. This figure shows that there is a peak in this ratio between 370 and 337 nm just as there is in the ratio $B(\nu)/A(\nu)$. We could not determine the exact position of this peak due to the fact that our laser cannot be tuned between 337 and 360 nm.

The time-integrated luminescence spectrum of the complex is also found to be dependent upon the excitation wavelength. This dependence upon excitation wavelength is also illustrated in Figure 1, where we have plotted the ratio of the luminescence intensity at 522 nm to the intensity at 486 nm. These wavelengths represent the first two maxima in the time-integrated luminescence spectrum of the complex. This ratio is found to decrease monotonically from 470 to 415 nm. At excitation wavelengths between 415 and 270 nm, the ratio remains constant within experimental error.

The dependence of the time-resolved luminescence spectrum of this complex on solvent is illustrated in Figure 4 for ethanol–methanol and methanol–water glasses. Although the spectra recorded at 50 μsec after excitation are nearly identical in the two solvent systems, the spectra which were recorded 2 μsec after excitation show a marked solvent dependence. Whereas the 2-μsec spectrum in ethanol–methanol has three well-resolved peaks at 486, 512, and 545 nm, only two peaks can be resolved in methanol–water at 495 and 527 nm.

Discussion

A. Analysis of Luminescence Decay Curves. The occurrence of a nonexponential luminescence decay curve for [$IrCl_2$(phen)(5,6-mephen)]Cl is indicative of several excited states which do not attain thermal equilibration. The rate of energy transfer between these states must therefore be comparable to or much less than the rate of return to the ground state. This in itself does not suggest that each of the states emits light, since a long-lived nonluminescent state which slowly feeds a shorter-lived emitting state could also lead to a nonexponential decay curve. However, the dependence of the shape of the luminescence decay curve for this complex on emission wavelength reveals that there are at least two nonequilibrated levels, each of which emits light.

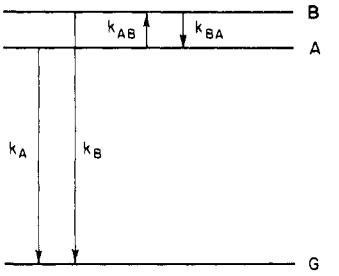

Figure 5. Two-level model for the emission of [$IrCl_2$(phen)(5,6-mephen)]Cl.

In a previous publication[6] it was suggested that the luminescence decay curves for this complex could be analyzed by assuming two emitting levels which do not attain thermal equilibration. We will analyze our results in terms of this model, but we wish to stress that our analysis may be generalized to more than two nonequilibrated emitting states.

The rate constants associated with the kinetic processes which we assume to occur in this model are depicted in Figure 5. In Figure 5, k_A represents the sum of the radiative and radiationless rate constants for conversion of the excited state, A, to the ground state, G. Rate constant k_B represents the analogous sum for conversion of the excited state, B, to the ground state, G. The constants k_{AB} and k_{BA} represent the rate of energy transfer between A and B. The excited states, A and B, may either be populated directly by absorption of light or indirectly by excitation of higher energy states which feed A and B by energy transfer processes. Although the relative concentrations of A and B will be dependent upon the wavelength of light used for excitation, we assume that these concentrations are established rapidly relative to the processes depicted in Figure 5.

The rates for depletion of the concentration of the two excited states are given by

$$-dn_B/dt = (k_B + k_{BA})n_B - k_{AB}n_A \quad (2)$$

$$-dn_A/dt = (k_A + k_{AB})n_A - k_{BA}n_B \quad (3)$$

The general solutions of these coupled differential equations have been presented by Zuclich et al.[9] and are given by

$$n_B(t) = c_{11}\exp(\lambda_1 t) + c_{12}\exp(\lambda_2 t) \quad (4)$$

$$n_A(t) = c_{21}\exp(\lambda_1 t) + c_{22}\exp(\lambda_2 t) \quad (5)$$

In the Zuclich treatment of this problem, the excited states are triplet sublevels and the constants, k_{AB} and k_{BA}, represent spin-lattice relaxation rates. In that situation, the excited levels are very close and both k_{AB} and k_{BA} are expected to be significant. In our case, the excited levels A and B are presumably electronic states of different orbital parentage,[6] and we assume that they are split by an energy gap which is large relative to kT at 77 K. We will present evidence to support this assumption at a later point. Proceeding on this assumption, we treat k_{AB} as a negligible quantity and eliminate the appropriate terms in eq 2 and 3. By introducing the initial conditions,

$$c_{11} + c_{12} = n_B{}^0 \quad (6)$$

$$c_{21} + c_{22} = n_A{}^0 \quad (7)$$

where $n_A{}^0$ and $n_B{}^0$ are the initial concentrations of states A and B, we obtain the following values for the λ's (exponential factors) and c's (pre-exponential factor):

$$\begin{aligned} \lambda_1 &= -k_B - k_{BA} \\ \lambda_2 &= -k_A \\ c_{11} &= n_B{}^0 \\ c_{12} &= 0 \end{aligned} \tag{8}$$

$$c_{21} = \frac{k_{BA}}{k_A - k_B - k_{BA}} n_B{}^0 \tag{9}$$

$$c_{22} = n_A{}^0 - \frac{k_{BA}}{k_A - k_B - k_{BA}} n_B{}^0$$

Substituting these results back into eq 4 and 5, we obtain the time dependence of the concentrations of A and B

$$n_B(t) = n_B{}^0 \exp[-(k_B + k_{BA})t] \tag{10}$$

$$n_A(t) = \left[n_A{}^0 - \left(\frac{k_{BA}}{k_A - k_B - k_{BA}} \right) n_B{}^0 \right] \exp(-k_A) + \left(\frac{k_{BA}}{k_A - k_B - k_{BA}} \right) n_B{}^0 \exp[-(k_B + k_{BA})t] \tag{11}$$

The total luminescence intensity, $I(\nu,t)$, measured in the determination of a decay curve will then be given by

$$I(\nu, t) = s[k_{BR} n_B(t) + k_{AR} n_A(t)] \tag{12}$$

where s is a proportionality constant and the constants k_{AR} and k_{BR} are the radiative rate constants for emission from levels A and B, respectively. Substitution of eq 10 and 11 into eq 12 leads to eq 13. This relation is of the form given

$$I(\nu,t) = sk_{AR}\left[n_A{}^0 - \frac{k_{BA}}{(k_A - k_B - k_{BA})} n_B{}^0 \right] \exp(-k_A t) + s\left[k_{BR} + k_{AR} \frac{k_{BA}}{k_A - k_B - k_{BA}} \right] n_B{}^0 \exp[-(k_B + k_{BA})t] \tag{13}$$

by eq 1 where τ_a is given by $1/k_A$ and τ_b is equal to $1/(k_B + k_{BA})$. The τ's are thus seen to represent the mean lifetimes of the two excited states. The preexponential factors, $A(\nu)$ and $B(\nu)$, are complex combinations of rate constants and initial concentrations.

In the more complex case when k_{AB} is not negligible, it can be shown that $I(\nu,t)$ still reduces to the general form given by eq 1. Furthermore, in the simplified case where both k_{AB} and k_{BA} are small relative to k_A and k_B, eq 1 still holds, and has a particularly simple interpretation. In this case, τ_a and τ_b are given by $1/k_A$ and $1/k_B$, while $A(\nu)$ and $B(\nu)$ represent the initial intensities, $I_A{}^0$ and $I_B{}^0$, of the two independent levels. Thus, eq 1 can be used to provide an empirical interpretation of the total luminescence decay curve from any two levels which fail to attain thermal equilibration, regardless of the degree to which the levels are uncoupled. Because of this, the purely empirical fit of our experimental luminescence decay curves provided by Table I does not provide any immediate way in which to determine the degree of coupling between the two levels in the model. However, a combination of additional experimental results can be used to provide an insight into the degree of coupling of the emitting levels.

Our most significant evidence which relates to the degree of coupling of these levels is contained in the dependence of our luminescence decay curves upon the excitation wavelength. The shape of the decay curve of $[IrCl_2(phen)(5,6\text{-mephen})]Cl$ is, within experimental error, a single exponential for excitation wavelengths in the region 450–505 nm. This shape is also insensitive to the emission wavelength monitored in the experiment. These observations indicate that a single level is predominantly excited and then luminesces under the conditions of the experiment. This leads us to the following two possible interpretations. (1) The dominant level excited under these conditions is the lowest excited level, A, and k_{AB} is indeed negligible as we have assumed. Under these circumstances $A(\nu)$ would be equivalent to $I_A{}^0$, $B(\nu)$ would be zero, and τ_a would be equal to the observed lifetime of 9.5 μsec for the nearly exponential decay. (2) The level excited under these conditions is the higher level, B, and both k_{AB} and k_{BA} are negligible. Under these circumstances, $B(\nu)$ would be equivalent to $I_B{}^0$, $A(\nu)$ would be zero, and τ_b would be equal to the observed lifetime of 9.5 μsec. In the following discussions we will show that our data support the latter interpretation.

It is important to note that in either case our experimental result fixes the value of one of the τ's at 9.5 μsec and confirms that k_{AB} is negligible. Although it is tempting to discard case (2) on the basis that long-wavelength excitation should lead to population of the lower rather than the upper level, a large difference in extinction coefficients for the two levels could lead to preferential population of the upper level under long-wavelength excitation. In view of the fact that the other value of τ used in fitting our nonexponential decay curves was 65 μsec, it is highly probable that the level with a lifetime 9.5 μsec has a shorter radiative lifetime and, hence, a larger extinction coefficient. Under higher energy excitation, the relative population of the two levels would no longer depend upon their extinction coefficients, but rather would be determined by the relative efficiencies of the radiationless processes responsible for feeding them.

It is significant to note that the τ value of 65 μsec is within experimental error of the luminescence lifetime of 66 μsec which has been reported for $[IrCl_2(5,6\text{-mephen})_2]Cl$ under identical experimental conditions.[10] It is quite likely that one of the luminescent levels of the heterobischelated complex should be similar in its character to the emitting level of $[IrCl_2(5,6\text{-mephen})_2]Cl$. However, an identical lifetime for this level in the two complexes would be expected only if the level is not coupled to a second level in the heterobischelated complex. Thus, the value of 65 μsec for the longer-lived level suggests that it does not feed the shorter-lived level, whereas the appearance of a nearly exponential decay under long-wavelength excitation for the shorter-lived level suggests that it does not feed the longer-lived level. Thus, there is strong evidence to conclude that both k_{AB} and k_{BA} are negligible. This is required by case (2), but is also consistent with case (1) since k_{BA} could be negligible in this case also.

As we have noted, if k_{BA} and k_{AB} are both negligible, $A(\nu)$ and $B(\nu)$ take on the physical significance of being the initial luminescence intensities, $I_A{}^0$ and $I_B{}^0$, of the two independent levels. In this case, it is possible to resolve the time-integrated luminescence spectrum of each of the levels. To do this we calculate the area under the decay curve for each of the components from the formulas

$$I_A(\nu) = \int_0^\infty I_A(\nu, t)dt = \int_0^\infty I_A{}^0(\nu) e^{-t/\tau_a} dt = I_A{}^0(\nu)\tau_a$$

$$I_B(\nu) = \int_0^\infty I_B(\nu, t)dt = \int_0^\infty I_B{}^0(\nu) e^{-t/\tau_b} dt = I_B{}^0(\nu)\tau_b \tag{14}$$

By use of (14) and the ratios $I_A{}^0/I_B{}^0$ given in Table I, we calculate the ratios $I_A(\nu)/I_B(\nu)$ throughout the emission spectrum. From the time-integrated total emission spectrum obtained by steady-state illumination at 337 nm, we can determine the sum of $I_A(\nu)$ and $I_B(\nu)$ at each frequency. From this information we solve for $I_A(\nu)$ and $I_B(\nu)$ and thereby obtain the emission spectrum of each of the two components. The results of this analysis are shown in Figure 6. Graphical integration of the emission intensities of each component over all frequencies yields a value of 0.25 for the

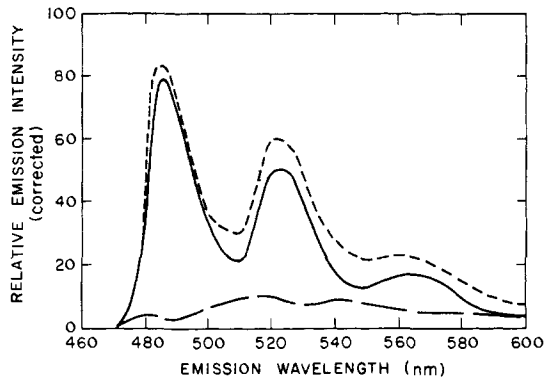

Figure 6. Time-integrated emission spectra of the emitting levels of [$IrCl_2$(phen)(5,6-mephen)]Cl generated by analysis of decay curves excited at 337 nm in ethanol–methanol (4:1 v/v) at 77 K: (—) emission spectrum of the 65-μsec lifetime level; (- - -) emission spectrum of the 9.5-μsec lifetime level; (- - -) total emission spectrum.

ratio of the short-lived to the long-lived emission intensity under 337-nm excitation.

It is significant to note that the highest energy peak in the emission spectrum of the short-lived component occurs at 480 nm whereas the first peak in the spectrum of the long component occurs at 486 nm. Assuming identical Stokes' shifts for the two components, this indicates that the short-lived component lies roughly 200–300 cm^{-1} above the long component. This energy gap is consistent with our assumption that k_{AB} is negligible, since it represents an unfavorable thermal barrier at 77 K. Furthermore, this confirms the formulation presented by case (2) which suggests that the short-lived state produced by low-energy excitation is, in fact, the uppermost of the two levels. On the basis of this analysis, we are now in a position to interpret the dependence of the ratio, $B(\nu)/A(\nu)$, on excitation wavelength which is presented in Figure 3. Since this represents the ratio of the initial populations of the two emitting levels, regions where the ratio becomes large correspond to increased efficiency for population of the 9.5-μsec level. Where the ratio becomes small, population of the 65-μsec level becomes more efficient. Thus, population of the short-lived level is favored by irradiation in the low-energy tail of the absorption spectrum and by irradiation between 370 and 337 nm.

B. Analysis of Time-Resolved Spectra. The emission spectra of the two levels presented in Figure 6 are markedly similar to the 2 and 400 μsec time-resolved spectra presented in Figure 2. According to our analysis, the 400-μsec spectrum should be nearly identical with the time-integrated spectrum of the long-lived component since only the 65-μsec component has any significant intensity 400 μsec after the initial excitation. Since 2 μsec is considerably shorter than the lifetime of either component, the spectrum taken at this delay time should resemble the sum of $A(\nu)$ and $B(\nu)$. The correspondence of this analysis with the time-resolved spectra in Figure 2 provides direct, experimental verification of the method we employed to determine the spectra in Figure 6.

On the basis of our resolution of the total emission spectrum of [$IrCl_2$(phen)(5,6-mephen)]Cl into the sum of the spectra of a long- and a short-lived component, we are now in a position to analyze the dependence of the time-resolved spectra of this complex on excitation wavelength. The relative growth of the 486-nm peak of the 2-μsec time-resolved spectrum with decreasing excitation wavelength between 472 and 337 nm is indicative of a relative increase in the initial population of the long-lived level over the short-lived level. This interpretation is consistent with the relative decrease in intensity and red shift of the peak which appears at 510 nm under 472-nm excitation, since, on the basis of Figure 6, this behavior would be expected as the relative population of the long-lived level over the short-lived level is increased.

From the preceding interpretation, the ratio of the emission intensity at 510 nm to the emission intensity at 486 nm in the 2-μsec time-resolved spectrum of [$IrCl_2$(phen)(5,6-mephen)]Cl provides a measure of the relative initial populations of the two emitting levels. Thus, where this ratio increases in Figure 1, an increase in the relative population of the short-lived level is indicated. It is interesting to note that the increase in this ratio between 370- and 337-nm excitation may be roughly correlated with a shoulder in the room-temperature absorption spectrum of the complex which occurs at about 375 nm. Excitation of the complex in the area of this shoulder and in the area where the low-energy tail of the absorption occurs therefore enhances the relative population of the short-lived level over the long-lived level.

Figure 1 also shows that the total luminescence spectrum of the complex under continuous irradiation contains evidence for enhanced population of the short-lived level at low excitation energies. However, the peak between 370 and 337 nm which was observed in the ratios taken from the time-resolved spectra is absent in the ratios taken from the time-integrated spectra. We attribute this to the fact that the total intensity carried by the short-lived component is only about one-quarter of that carried by the long-lived component in the time-integrated spectrum. Under these conditions, small increases in population of the short-lived component cannot be detected. On the other hand, both components contribute to the 2-μsec time-resolved spectrum with similar intensities, and smaller changes in the relative populations of the two levels become detectable.

The dependence of our time-resolved spectra on the solvent medium provides evidence to support our previous claim that the emitting levels arise from different orbital parentage.[6] Since the spectra recorded at 50 μsec after excitation show no sign of solvent dependence, we conclude that the long-lived level probably has primarily a $\pi\pi^*$ orbital parentage. The dependence of the 2-μsec spectra in Figure 4 on solvent indicates that the energy of the short-lived level is affected by the solvent polarity. Although the high-energy peak of the 2-μsec spectrum is shifted to *lower energy* when the solvent polarity is increased, this is probably due to a shift of the short-lived level to *higher energy* (vide infra). Since the energy of the long-lived component is not dependent on solvent, the 486-nm peak observed in ethanol–methanol remains at this wavelength in methanol–water (see Figure 4). However, the most intense band in the luminescence of the short-lived component appears at 515 nm, and a shift of this band to higher energy would cause it to merge with the 486-nm peak of the long-lived component in methanol–water. This shift of the short-lived level to higher energy in methanol–water indicates that its orbital parentage includes a significant $d\pi^*$ contribution.

We see no sign of the low-intensity peak of the short-lived component which appears at 480 nm in ethanol–methanol when the solvent is changed to methanol–water. Although this peak could be resolved only by our decay curve analysis and not by time-resolved spectroscopy in ethanol–methanol, one might expect time-resolved spectroscopy to show an indication of its presence if its shifts to shorter wavelengths. Our inability to detect this peak via time-resolved spectroscopy may be due to its low intensity. Alternatively, this peak may be due to the presence of a third level whose energy is not affected by solvent polarity. This alternative is also suggested by the fact that the most seri-

ous deviations from the curve-fitting procedure which was employed for analysis of decay curves were found between 474 and 484 nm. The possible contribution of a third level to the emission of this complex is currently being studied.

Summary

To clarify the interrelationships among the various data presented, we now summarize our experimental observations and the direct conclusions we have obtained from them.

1. It was found that excitation wavelengths greater than 450 nm give simple exponential luminescence decay curves and an observed lifetime of 9.5 ± 0.4 μsec.

2. Using this independently measured lifetime as τ_b in eq 1, the best nonlinear least-squares fit to the decay curve data measured as a function of emission wavelength (Table I) was found for $A(\nu)$ and $B(\nu)$ when τ_a is chosen to be 65 μsec.

3. From a plot of the resulting intensities, $A(\nu)$ and $B(\nu)$, vs. emission wavelength (Figure 6) it is evident that the state characterized by $B(\nu)$ and τ_b = 9.5 μsec has a high-energy emission maximum near 480 nm; whereas the state characterized by $A(\nu)$ and τ_a = 65 μsec has a high-energy maximum near 486 nm.

Hence the short-lived state corresponds to state B in Figure 5, the long-lived state corresponds to state A, and the energy gap between them is around 200–300 cm^{-1}. These assignments are reinforced by the observed similarity between the long-lived emission spectrum of state A in Figure 6 and the 200-μsec time-resolved spectrum in Figure 2, and by the contrasting general appearance of the 2-μsec time-resolved spectrum in Figure 2, noting especially the short-wavelength shoulder which grows in.

4. For long delay times, 50 μsec or longer, change in solvent polarity had a negligible effect on the time-resolved luminescence spectrum.

However, the 2-μsec time-resolved spectra showed a significant solvent shift (Figure 4), strongly suggesting that the short-lived component is the one affected.

The combined observations on luminescence lifetimes and on solvent dependence of emission energies strongly indicate the assignment of state A as a $\pi\pi^*$ ligand-localized excited state (long lifetime, negligible solvent dependence) and the assignment of state B as a $d\pi^*$ charge transfer excited state (short lifetime, marked solvent dependence).[10]

5. In addition to the observation that >450-nm excitation almost exclusively gives the short-lived emission, decay curve analysis has shown that component intensities are complicated functions of excitation wavelength throughout the attainable range of light absorption by the complex (Figure 1).

6. Similarly, the 2-μsec time-resolved luminescence spectra have shown a complicated dependence on the wavelength of light absorbed (Figure 1) in the ratio of 510-nm intensity to 486-nm intensity. The excitation wavelength dependence of the luminescence indicates that the level initially excited by the laser selectively depopulates into one or the other emitting state. Hence, selective population of state B by excitation in the 337–370-nm region is strongly indicated by observed peaks in the intensity ratios plotted in Figure 1. This suggests that these are definite selection rules which govern the radiationless deactivation pathways in the complex.

Concluding Remarks

The similarity of the energy and lifetime of the long-lived emitting level of this complex with the luminescent state of $[IrCl_2(5,6\text{-mephen})_2]Cl$[10] is remarkable. This similarity indicates that the level with $\pi\pi^*$ orbital parentage is localized in the part of the complex which contains the 5,6-mephen ligand. Although our evidence indicates that the second level has a $d\pi^*$ orbital parentage, the nature of this level is somewhat obscure at this point. Our two-level analysis places this level 200–300 cm^{-1} *above* the $\pi\pi^*$ level, but a three-level model may place another short-lived level *below* the $\pi\pi^*$ level.

Several other simple alternatives for the nature of the short-lived level should also be considered. One possibility would be a charge transfer from iridium(III) to a π^* orbital delocalized over both the phen and 5,6-mephen ligands. Another alternative would be a transfer of charge from one of the bidentate ligands to the other. Although this would technically be a $\pi\pi^*$ state, we would expect it to have many of the characteristics of a $d\pi^*$ level since it would involve the transfer of charge over a relatively large distance. A final alternative may be that the short-lived level has large contributions from both $d\pi^*$ and $\pi\pi^*$ configuration, and is similar to the emitting level of $[IrCl_2(4,7\text{-mephen})_2]Cl$.[10] Each of these alternatives is faced with the difficulty that the short-lived level is depicted as involving the delocalization of charge density over both bidentate ligands. This point of view is difficult to reconcile with our evidence that the short-lived level is not coupled to a $\pi\pi^*$ level localized in the 5,6-mephen part of the complex by any radiationless process. Rather, we would expect a lack of radiationless coupling of two levels to be an indication that the excitation is localized in different parts of the complex.

Our analysis of the dependence of the luminescence decay curves for this complex on the excitation wavelength indicates that the relative efficiencies of the radiationless processes which feed these two levels are dependent upon the nature of the higher level. Excitation of the complex between 370 and 337 nm produces an upper level which feeds the short-lived state with enhanced efficiency. This region correlates roughly with a region in the absorption spectrum where a charge transfer peak occurs.[6] Thus, our results suggest that excitation of high-energy charge transfer states favors charge transfer emission whereas excitation of high-energy $\pi\pi^*$ states favor $\pi\pi^*$ emission. It appears, therefore, that the paths of radiationless deactivation in this complex tend to favor a retention of the orbital nature of state produced by excitation. This suggests a set of selection rules for radiationless transitions in this complex which are based on the orbital parentage of the levels. These rules may be formulated as follows: $d\pi^* \nleftrightarrow d\pi^*$; $\pi\pi^* \nleftrightarrow \pi\pi^*$; $d\pi^* \nleftrightarrow \pi\pi^*$.

In our formulation of these selection rules, we have purposely avoided any indication of spin multiplicities. Recent studies of the splittings of sublevels of excited states of heavy-metal complexes suggest that spin–orbit coupling is so large that the classification of states by spin multiplicities is of little use.[11] Although future studies may disclose further selection rules based upon the total symmetry properties of individual sublevels, we feel that our results are best formulated in terms of the overall orbital parentage. In this formulation, each level of $d\pi^*$ and $\pi\pi^*$ orbital parentage is likely to consist of several thermally equilibrated sublevels.

At the present time, our results do not provide any evidence which implicates d–d levels in the radiationless deactivation pathways for this complex. However, the complexes $[IrCl_2(phen)_2]Cl$ and $[IrCl_2(5,6\text{-mephen})_2]Cl$ are known to undergo photochemical aquation,[12] and d–d levels have been implicated in the aquation process. It is therefore quite likely that d–d levels are populated and depopulated in the radiationless deactivation pathways for $[IrCl_2(phen)(5,6\text{-mephen})]Cl$. Unfortunately, we have no evidence upon which to suggest a set of selection rules for radiationless transitions involving d–d levels.

We feel that the set of orbital selection rules for radiationless transitions which appear to operate in this complex are only a rough guideline to help indicate which radiationless processes are more and less favorable. For any two given states, vibrational factors as well as factors based upon the orbital nature of the levels will be important in determining the rate of energy transfer between them. It may very well be that in this particular complex, both the orbital and vibrational factors are unfavorable for fast radiationless transitions. In other complexes, it may happen that the vibrational factors are large enough to cause rapid radiationless transitions even though the orbital parentage of the levels may be unfavorable for these processes. Since the vibrational factors which govern radiationless processes are dependent upon the energy gaps between the levels, it may be that the energy gaps between levels of different orbital parentage are particularly unfavorable in $[IrCl_2(phen)(5,6\text{-mephen})]Cl$. We will explore the implications of our proposed selection rules for radiationless transitions in a later publication. At that time we will also report experimental studies of energy transfer in other hetereobischelated complexes of Ir(III).[13]

Acknowledgment. Acknowledgment is made to the donors of The Petroleum Research Fund, administered by the American Chemical Society, for support of this research.

References and Notes

(1) NSF-URP Undergraduate Research, Associate, Summer 1974.
(2) (a) J. N. Demas and G. A. Crosby, *J. Am. Chem. Soc.*, **92**, 7262 (1970); **93**, 2841 (1971); M. K. DeArmond, *Acc. Chem. Res.*, **7**, 309 (1974); R. J. Watts and G. A. Crosby, *J. Am. Chem. Soc.*, **94**, 2606 (1972); (b) R. J. Watts, R. W. Harrigan, and G. A. Crosby, *Chem. Phys. Lett.*, **8**, 49 (1971); R. W. Harrigan, G. D. Hager, and G. A. Crosby, *ibid.*, **21**, 487 (1973); R. W. Harrigan and G. A. Crosby, *J. Chem. Phys.*, **59**, 3468 (1973); K. W. Hipps and G. A. Crosby, *Inorg. Chem.*, **13**, 1544 (1974).
(3) J. D. Petersen and P. C. Ford, *J. Phys. Chem.*, **78**, 1144 (1974); G. Malouf and P. C. Ford, *J. Am. Chem. Soc.*, **98**, 601 (1974); P. C. Ford, University of California, Santa Barbara, private communication.
(4) J. L. Kelly and J. F. Endicott, *J. Am. Chem. Soc.*, **94**, 1797 (1972).
(5) W. Halper and M. K. DeArmond, *J. Lumin.*, **5**, 225 (1972).
(6) R. J. Watts, *J. Am. Chem. Soc.*, **96**, 6186 (1974).
(7) G. A. Crosby, Washington State University, private communication.
(8) R. J. Watts and J. S. Harrington, *J. Inorg. Nucl. Chem.*, **37**, 1293 (1975).
(9) J. Zuclich, J. U. von Schütz, and A. H. Maki, *Mol. Phys.*, **28**, 33 (1974).
(10) R. J. Watts, G. A. Crosby, and J. L. Sansregret, *Inorg. Chem.*, **11**, 1474 (1972).
(11) G. A. Crosby, K. W. Hipps, and W. H. Elfring, Jr., *J. Am. Chem. Soc.*, **96**, 629 (1974).
(12) R. Ballardini, G. Varani, L. Moggi, V. Balzani, K. R. Olson, F. Scandola, and M. Z. Hoffman, *J. Am. Chem. Soc.*, **97**, 728 (1975).
(13) R. J. Watts, B. G. Griffith, and J. S. Harrington, *J. Am. Chem. Soc.*, in press.

Kinetics of the Reduction of *Rhus vernicifera* Laccase by Ferrocyanide Ion

Robert A. Holwerda and Harry B. Gray*

Contribution No. 5026 from the Arthur Amos Noyes Laboratory of Chemical Physics, California Institute of Technology, Pasadena, California 91125. *Received December 14, 1974*

Abstract: Kinetic studies of the reduction of *Rhus vernicifera* laccase by ferrocyanide ion are reported, and the results are compared with previous findings for hydroquinone as reductant. Observed rate constants for reduction of the laccase "blue" and ESR nondetectable copper sites are identical to within experimental error, and vary with $[Fe(CN)_6^{4-}]$ in a complicated fashion. Relaxation rate data are reported for runs in which laccase was mixed with solutions containing comparable concentrations of ferro- and ferricyanide ions. These results establish that a reversible one-electron transfer from $Fe(CN)_6^{4-}$ to the "blue" copper atom occurs: $Fe(CN)_6^{4-}$ + type 1 Cu(II) $\rightleftharpoons$ $Fe(CN)_6^{3-}$ + type 1 Cu(I) ($k_1 = 24.9\ M^{-1}\,sec^{-1}$, $k_{-1} = 26.8\ M^{-1}\,sec^{-1}$; pH 6.9, $\mu = 0.2$, 25.1°). Comparisons between aerobic ferrocyanide turnover rates and laccase reduction rate constants reveal that four electrons are released to oxygen at a rate proportional to the velocity of the initial laccase reduction step. Fluoride ion fails to inhibit the reaction between ferrocyanide ion and laccase at pH 7.0. The pH dependence results show that a 23-fold laccase reduction rate decrease accompanies ionization of one or more amino acid residues with $pK = 6.41$. It is suggested that the involved residue is histidine, and that ion-pair formation between the highly charged reductant and imidazolium cations may be an integral part of the "blue" copper reduction mechanism. Ionic strength dependence results are in accord with the latter hypothesis.

Laccases are versatile copper-containing enzymes that catalyze the oxidation of a wide variety of phenolic substrates by oxygen, producing quinones, phenol coupling products, and water as the sole oxygen reduction product.[1] Spectroscopic studies of fungal and lacquer tree laccases have revealed that both enzymes possess four tightly bound copper atoms incorporated into "blue" (type 1), ESR detectable, optically nondetectable (type 2), and ESR nondetectable (type 3, 2 Cu/mol) sites.[2] We have undertaken kinetic studies of the reduction and oxidation of *Rhus vernicifera* laccase as part of a program aimed at elucidating biochemical mechanisms for the fixation and reduction of molecular oxygen. Our previously reported stopped flow study of the anaerobic reduction of laccase by hydroquinone[3] suggested that inner-sphere complexes between the phenolate monoanion (HQ^-) and type 2 Cu(II) are intermediates in closely related electron transfer pathways to the type 1 and type 3 copper sites. It was further proposed that the disposition of these intermediates involves (1) reduction of the type 2 copper atom followed by intramolecular electron transfer to the type 3 site, and (2) initiation of a protein conformational change permitting conduction of an electron from the coordinated substrate to the type 1 copper atom. For comparison with the hydroquinone reduction results, we report here our kinetic observations for the reaction between laccase and a one-electron inorganic reductant, ferrocyanide ion, which typically participates in outer-sphere electron transfer reactions.